INSTITUTE OF PHYSICS PUBLISHING JOURNAL OF OPTICS B: QUANTUM AND SEMICLASSICAL OPTICS

J. Opt. B: Quantum Semiclass. Opt. **7** (2005) S158–S165 doi:10.1088/1464-4266/7/7/005

Semiconductor sources of twin photons for quantum information

S Ducci[1], L Lanco[1], Y Seurin[1], G Leo[1], V Berger[1], A De Rossi[2] and X Marcadet[2]

[1] Laboratoire Matériaux et Phénomènes Quantiques, UMR 7162, Université Paris 7—Denis Diderot, 2, Place Jussieu, Case 7021, 75251 Paris, France
[2] Thales Research and Technology, Domaine de Corbeville, 91404 Orsay, France

Received 18 January 2005, accepted for publication 23 March 2005
Published 30 June 2005
Online at stacks.iop.org/JOptB/7/S158

Abstract

A large number of scientific proposals made in the last few years are based on transport and manipulation of information using single quantum objects. Some of them make use of entanglement in pairs of particles such as twin photons.

Although theoretical proposals have demonstrated highly interesting perspectives in the quantum information domain, experimental realizations and applications still suffer from the complexity of experimental set-ups and technological limitations.

This paper presents various approaches aiming at efficient twin photon semiconductor sources. The emergence of these compact and integrated devices would be an important technological breakthrough in quantum information applications.

Keywords: nonlinear waveguides, frequency conversion, semiconductor materials

(Some figures in this article are in colour only in the electronic version)

1. Introduction

The number of scientific proposals based on transport and manipulation of information using single quantum objects has grown considerably in recent years. Impressive theoretical perspectives have been envisaged in many domains of quantum information (computation [1], teleportation [2, 3], cryptography [4], metrology [5]); nevertheless, experimental demonstrations and practical applications are still limited due to technological difficulties with present state-of-the-art devices (sources, detectors, fibred or free space transmission, optical elements).

In this paper we are concerned with the problem of sources: many of the quantum information protocols proposed up to now are based on the availability of sources of twin photon pairs; this kind of source can be used in single photon protocols (one photon is used to transport the quantum information and its twin to trigger a detector only when it is necessary, thus improving the signal to noise ratio) as well as in protocols that use the entanglement properties of the pair (polarization, energy–time, time–bin).

The most widely used means to produce photon pairs is parametric down-conversion, in which a photon with a frequency ω_p, interacting with a nonlinear material, creates twin photons with frequency ω_i and ω_s such that $\omega_p = \omega_i + \omega_s$. The first kind of materials used to generate twin photons were birefringent nonlinear crystals; however the utilization of bulk crystals neither allows one to obtain high conversion efficiencies nor allows one to have an efficient collection of generated photons. The best way to solve these problems is to implement the down-conversion process in nonlinear waveguides. So far, the fabrication of periodically poled lithium niobate waveguides has permitted us to reach conversion efficiencies up to 10^{-6} [6]. Semiconductors represent another 'privileged' material for achieving twin photon sources, as they present huge nonlinearities and they are laser materials; these potentialities open the possibility to realize integrated sources which could become important devices in the toolbox of quantum information experiments.

In this paper we present our latest advances in semiconductor twin photon sources. The materials used are GaAs and AlGaAs, their growth techniques being well

mastered. An important condition to satisfy to have an efficient down-conversion process is the momentum conservation of the interacting photons. Whereas in bulk crystals this is usually obtained thanks to natural birefringence, GaAs is isotropic and alternative schemes of phase matching have to be used.

The remainder of this paper is organized as follows: in sections 2–4 we report the results obtained with devices based on form birefringence, modal phase matching, and counterpropagating signal and idler respectively; in section 5 we discuss and compare the characteristics of these three kinds of devices.

2. Form birefringence phase matching

Form birefringence phase matching is achieved by using the artificial birefringence of a composite multilayer material: the isotropy of bulk GaAs is broken by inserting thin oxidized AlAs (Alox) layers in GaAs. The idea has been proposed in a pioneering paper of Van de Ziel in 1975 [7], but the experimental realization of form birefringence phase matching was achieved only in 1997, when the development of oxidation techniques [8] permitted the realization of a well suited couple of materials having a high nonlinear coefficient, and a high enough refractive index contrast was found [9].

The principle of form birefringence can be understood by making some symmetry considerations on the crystalline structure on this new artificial material. The presence of thin Alox layers grown on a (100) GaAs substrate breaks the symmetry of threefold rotation axes of the GaAs and the point group of the composite material becomes $\bar{4}2m$, the same as for KDP. In this way we obtain a material with the same nonlinear properties as GaAs (the small zero contribution of the thin Alox layers can be neglected), and the linear optical properties of KDP.

For a periodic layered medium and a propagation direction as sketched in figure 1 (upper part), it can be shown that

$$n_{\mathrm{TE}}^2 = \frac{h_1}{\Lambda} n_1^2 + \frac{h_2}{\Lambda} n_2^2$$

$$\frac{1}{n_{\mathrm{TM}}^2} = \frac{h_1}{\Lambda}\frac{1}{n_1^2} + \frac{h_2}{\Lambda}\frac{1}{n_2^2}$$

with Λ the period and h_i (n_i) the thickness (refractive index) of the ith repeated layer ($i = 1, 2$; $h_1 + h_2 = \Lambda \ll \lambda$). Form birefringence ($n_{\mathrm{TE}}$–$n_{\mathrm{TM}}$) occurs due to different boundary conditions for E_{TE} and E_{TM}, and increases with the index contrast of the two materials as shown in figure 1 (lower part).

With such waveguides, difference frequency generation (DFG) [10], second harmonic generation (SHG) [11] and parametric fluorescence (PF) [12] have been reported. Hereafter, we detail the results obtained for PF which is an interesting process for obtaining twin photons.

The sample used for PF is grown by molecular beam epitaxy on a GaAs(001) substrate. Its epitaxial structure is the following: 1000 nm AlAs/1000 nm $Al_{0.7}Ga_{0.3}As$/4× (37 nm AlAs/273 nm GaA)/37 nm AlAs/1000 nm $Al_{0.7}Ga_{0.3}As$/30 nm GaAs. This structure is designed such that, after oxidation, a type I degenerate three wave mixing at about 1064 nm (pump wavelength) is obtained. A CW Ti:Sa laser tunable from 950 to 1070 nm is coupled into a 3.2 mm long waveguide with a piezoelectric positioner and a standard 40× microscope

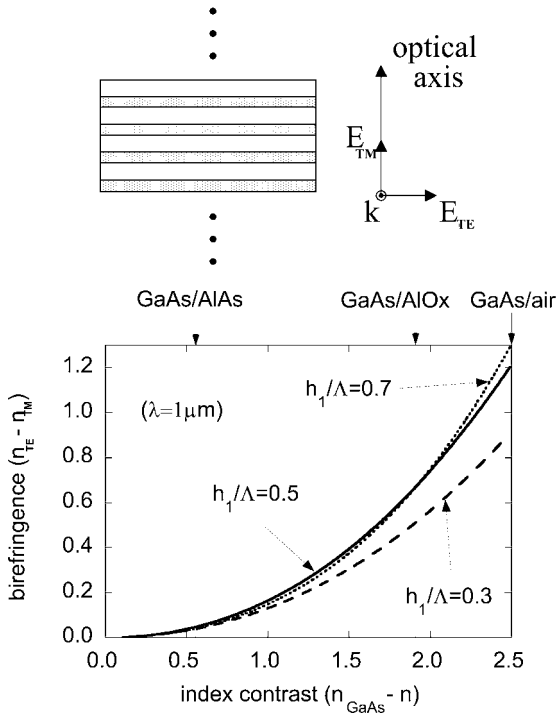

Figure 1. Form birefringence in a stack of GaAs layers alternated with a material of index n.

objective. The PF signal is detected with a InSb detector, the pump being completely absorbed by a germanium filter. As expected from the selection rules imposed from crystal symmetry and phase matching, the signal and idler are TE polarized for a TM polarized pump. Due to the spectral broadening at degeneracy, typical of a type I process, we expect the spectrally integrated PF output to increase rapidly as the degeneracy is approached, whereas at longer pump wavelength almost no photons are generated because phase matched down-conversion is forbidden. The corresponding measurement is shown in figure 2, where the PF peak appears clearly and its shape is asymmetric with a sharp fall on the right-hand side. It has also been shown that the output signal power depends linearly on the pump power [12], as expected in the low gain limit of a PF process. Figure 3 shows the temperature dependence of signal/idler wavelengths for a given pump wavelength. In the calculated curve, temperature variation of the waveguide effective indices is deduced by using the Gehrsitz model [13].

The measurement of the normalized PF efficiency, defined as the amount of power carried by the signal wave divided by the waveguided pump power and normalized to the square of the sample length L, has given $\eta_{\mathrm{PF}} = 6 \times 10^{-6}$ W W^{-1} cm^{-2}.

The insulating nature of the oxidized layers of the Alox-based device prevents the achievement of a highly compact electrically pumped device. A high degree of compactness is possible with another kind of heterostructure, based on modal phase matching, which is described in the next section.

3. Modal phase matching

In the modal phase matching scheme phase velocity mismatch is compensated by multimode waveguide dispersion, without

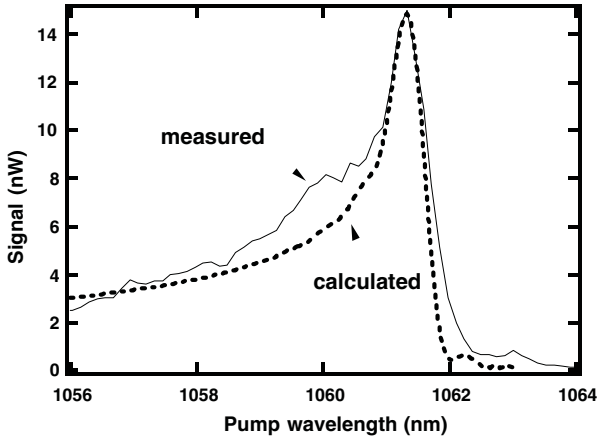

Figure 2. Parametric fluorescence signal versus pump wavelength.

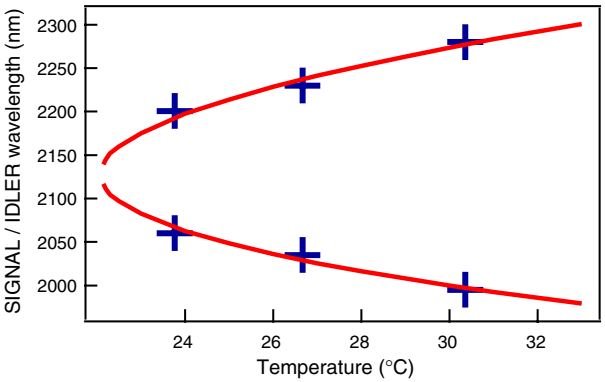

Figure 3. Signal/idler wavelength versus temperature, for $\lambda_p = 1.064$ μm: experimental points (crosses) and calculated curve. Experimental twin points correspond to a single measurement: one energy has been measured, and the other one has been reported considering energy conservation.

requiring any oxidation process. An important advantage of this solution is therefore its compatibility with an electrically pumped laser, which allows one to integrate lasing action and nonlinear effects. Our device is designed such that the effective index of the third order guided mode (TE_{20}) at 775 nm is the same as that of the fundamental modes (TE_{00} and TM_{00}) at 1.55 μm. As a consequence, this configuration allows the parametric generation of twin photons at 1.55 μm, starting from photons at 775 nm in the third order mode [14].

Figure 4 shows the dispersion of the effective indices n_{eff} for the modes involved in the frequency conversion process.

A quantum well is inserted inside the waveguide in order to provide the lasing action on the third order mode; this internal source for the parametric down-conversion endows this device with two main advantages: a high degree of compactness and the absence of pump coupling losses [15].

The design of this heterostructure stems from several constraints.

(1) It is necessary to optimize the nonlinear overlap integral to have a good conversion efficiency. For this reason we choose a third order mode instead of a second order one.
(2) It is necessary to insert inside the structure a quantum well emitting on the third order mode; this means that the third order mode has to have a strong overlap with the quantum well, whereas the fundamental mode has to be weak. This condition can be satisfied by designing a heterostructure as shown in the inset of figure 4. The peculiarity of this structure resides in the presence of the two 'barrier layers' which further the third order mode with respect to the fundamental one at the quantum well location (the electric field of the fundamental is reduced in the centre of the structure by these two low index layers).
(3) Too high energy barriers at the hetero-interfaces should be avoided, as these could block the carrier transport towards the quantum well thus hindering the necessary radiative recombination.
(4) It is also necessary to accurately optimize the refractive indices of the heterostructure layers to improve mode confinement thus reducing optical losses.

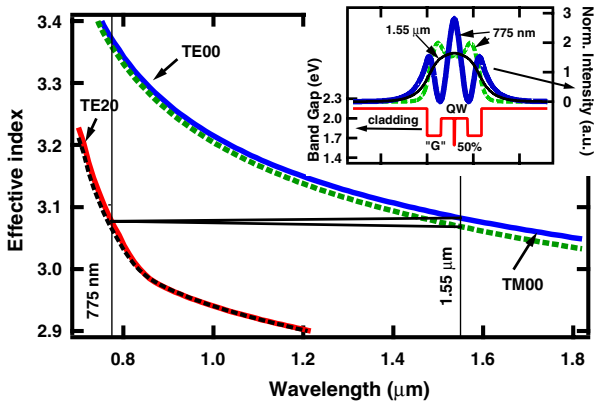

Figure 4. Calculated effective indices of the guide modes of the sample as a function of wavelength. The triangle joining TE_{20} at 775 nm and TE_{00} and TM_{00} curves at 1.55 μm illustrates the phase matching condition. Inset: band gap profile and intensity distribution of the modes TE_{20} at 775 nm and TE_{00} and TM_{00} at 1.55 μm. In the band gap profile are shown the cladding and the waveguide core, entailing the 'G' layers ($Al_{0.25}Ga_{0.75}As$), the 'barrier layers' ($Al_{0.5}Ga_{0.5}As$) and the quantum well.

A subtle trade-off of all these constraints has recently allowed the realization of an electrically pumped laser device [15].

The laser diode is grown by molecular beam epitaxy on a GaAs substrate and processed for gain-guided operations. The epitaxial structure used is 1200 nm $Al_{0.98}Ga_{0.02}As$ (cladding)/152 nm $Al_{0.25}Ga_{0.75}As$ (generation layer)/138 nm $Al_{0.50}Ga_{0.50}As$ (barrier layer)/10 nm $Al_{0.11}Ga_{0.89}As$ (quantum well)/138 nm $Al_{0.50}Ga_{0.50}As$ (barrier layer)/152 nm $Al_{0.25}Ga_{0.75}As$ (generation layer)/1200 nm $Al_{0.98}Ga_{0.02}As$ (cladding). The current aperture is realized by proton implantation into the upper cladding layer and ohmic contacts are deposited afterwards. The waveguide core is uniformly doped at 2×10^{17} cm^{-3}; the cladding layers are gradually doped from 2×10^{17} to 10^{18} cm^{-3}.

Figure 5 shows an image of the diode laser on its mount and the projection of the far field onto a screen: the emission on the third order is evident.

In order to demonstrate the presence of parametric effects inside the waveguide, a second harmonic generation (SHG) experiment has been realized on a sample having the same structure but without quantum well (in order to avoid the light absorption) [16]. The light of a CW Tunics Laser, tunable from

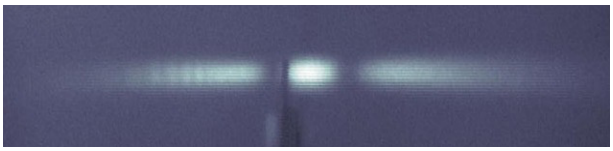

Figure 5. Image of the laser diode on its mount and the far field projected onto a screen.

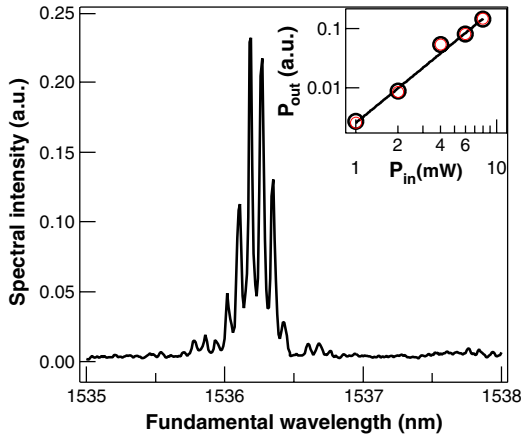

Figure 6. Typical SHG spectrum as a function of the fundamental wavelength. Inset: second harmonic output integrated power as a function of the fundamental input power on a log–log scale. Circles: experimental data. Solid line: squared power law fitting function $y \propto x^{1.99}$.

1.5 to 1.6 μm and with a spectral width of 2 kHz, is coupled to the waveguide via a 40× objective. The SHG signal is collected by a second 40× objective and detected with a p–i–n silicon photodiode connected to a lock-in amplifier. The input beam is linearly polarized at 45° in order to couple TE and TM modes simultaneously.

Figure 6 shows the intensity of the generated signal as a function of the pump wavelength.

An analyser inserted before the detector permits one to determine that the generated signal is TE polarized, which demonstrates that the observed SHG is a type II process.

The signal has a $(\sin x/x)^2$ shape, which is the signature of a phase matching resonance. In our case the signal is modulated by a Fabry–Perot transmission function as the fundamental beam is subjected to multiple reflections from the waveguide facets.

The internal SHG efficiency has been estimated to be $\eta = 30\% \pm 5\%$ W^{-1} cm^{-2}. This value is smaller than the one obtained in section 2 for two main reasons: firstly, the nonlinear overlap is smaller in the present modal phase matching scheme (where the interacting modes are the third and the first order modes); secondly, the third order mode may present important optical losses (which are not taken into account in the efficiency estimation) due to a bad confinement or to the presence of defects in the cladding layer.

From the SHG efficiency we can deduce the PF efficiency with the formula $\eta_{\mathrm{PF}} = \frac{P_{\mathrm{PF}}}{P_{\mathrm{P}} L^2} = \eta P_0$ [16], where P_0 is the vacuum fluctuation power, which depends on the bandwidth of the process. Since here the latter is estimated as around 15 THz, we expect $\eta_{\mathrm{PF}} \sim 6 \times 10^{-7}$ W W^{-1} cm^{-2}.

The observation of a PF signal requires that the laser emission wavelength (λ_{em}) corresponds to the phase matching (λ_{PM}). This condition can possibly be satisfied by using temperature as a parameter to tune the two wavelengths. Unfortunately, for the sample described in this section, it is not possible to satisfy the condition $\lambda_{\mathrm{em}} = \lambda_{\mathrm{PM}}$ for a temperature value which allows a good laser operation, and for this reason we have not measured a PF signal yet. It is clear that an important point for our devices is their sensitivity to the variations of the structure parameters. In particular, as shown in section 5, form birefringent and mode matched devices are quite sensitive to the layer thicknesses,. A much more stable device, based on a counterpropagating signal/idler geometry, is presented in the next section.

4. Counterpropagating signal and idler phase matching

The last phase matching scheme we present here rests upon the generation of guided wave counterpropagating signal and idler in the waveguide, from a pump beam which transversely illuminates the waveguide [17, 18]. Three kinds of semiconductor materials are currently studied in our group: AlGaAs for down-converted photons around 1.55 μm [19], and GaN and ZnSe for an emission around 800 nm [20]. All these materials lead to type II parametric interactions, where one of the down-converted photons is TE polarized, and the other one is TM polarized. This implies that there are two ways to cancel the phase mismatch in the z direction $\Delta k = k_{\mathrm{P}} \sin\theta + k_{\mathrm{I}} - k_{\mathrm{S}}$: either the signal is TE polarized and the idler is TM polarized (which we shall refer to as 'interaction 1'), or the signal is TM polarized and the idler is TE polarized ('interaction 2'). In figure 7 the two possible interactions are shown.

The central frequencies for the signal and the idler are determined through the conservation of energy and of momentum in the z direction, leading to the following equations:

$$\begin{aligned} &\omega_{\mathrm{P}} = \omega_{\mathrm{S}} + \omega_{\mathrm{I}} \\ &\omega_{\mathrm{P}} \sin\theta = \omega_{\mathrm{S}} n_{\mathrm{TE}}(\omega_{\mathrm{S}}) - \omega_{\mathrm{I}} n_{\mathrm{TM}}(\omega_{\mathrm{I}}) \end{aligned} \quad \text{(interaction 1)}$$

$$\begin{aligned} &\omega_{\mathrm{P}} = \omega_{\mathrm{S}} + \omega_{\mathrm{I}} \\ &\omega_{\mathrm{P}} \sin\theta = \omega_{\mathrm{S}} n_{\mathrm{TM}}(\omega_{\mathrm{S}}) - \omega_{\mathrm{I}} n_{\mathrm{TE}}(\omega_{\mathrm{I}}) \end{aligned} \quad \text{(interaction 2).}$$

These central frequencies obviously depend on the incidence angle θ of the pump beam, which provides a very convenient means to tune them.

In the x direction, the phase mismatch is simply $k_{\mathrm{P}} \cos\theta$ and thus cannot be perfectly cancelled. In order not to be limited to waveguide thicknesses lower than the pump wavelength, we use a quasi-phase matching technique by designing the core of the waveguides as an alternation of $\lambda_{\mathrm{P}}/2$ layers with $\chi^{(2)}$ nonlinear coefficients as different as possible.

We have implemented a numerical model in order to evaluate the main characteristics of various structures of the waveguide as θ is changed: the central frequencies of signal and idler, their modal profiles, their spectral widths, the propagation of the pump beam through the structure and the efficiency of the process.

Figure 8 reports the dependence of the signal and idler wavelengths on θ for a structure having the following epitaxial structure: 1081 nm $Al_{0.94}Ga_{0.06}As$ (cladding)/110 nm $Al_{0.25}Ga_{0.75}As$/4× [128 nm AlAs/110 nm $Al_{0.25}Ga_{0.75}As$] (core)/1081 nm $Al_{0.94}Ga_{0.06}As$ (upper cladding).

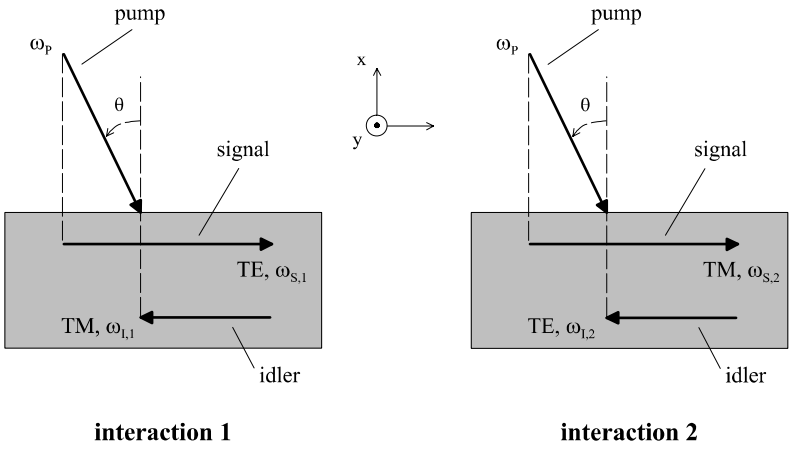

Figure 7. Wavevectors of the three interacting beams, for the two possible interactions with a fixed angle of incidence of the pump in the counterpropagating PF geometry.

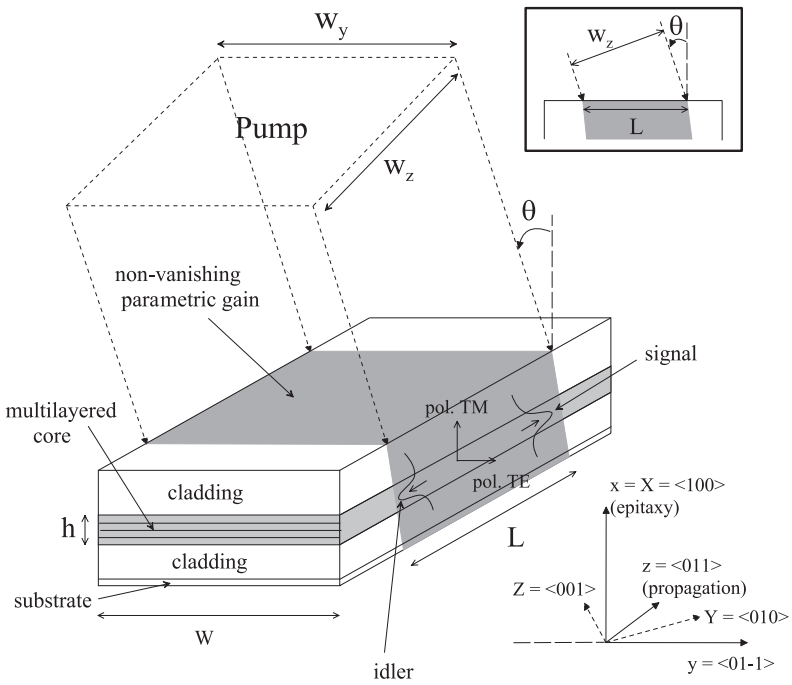

Figure 8. Schematic diagram of an AlGaAs waveguide with a pump beam at an angle of incidence θ. The two possible polarizations for the guided signal and idler are also represented. The core has a multilayered structure in order to achieve quasi-phase matching for the pump beam in the vertical direction. The inset is a lateral view of the waveguide.

We observe that X-shaped tuning curves occur, as expected in type II interactions; the difference between the degeneracy angles relative to interactions 1 and 2 is due to the modal birefringence in the waveguide.

The spectrum of the down-converted photons is given by the usual function $\mathrm{sinc}^2(\Delta kL/2)$, where L is the waveguide length. One of the main advantages of counterpropagating geometry arises from the rapid increase of Δk when one moves off from perfect phase matching, which leads to a very narrow bandwidth for the down-converted photons. This is favourable for this device, as chromatic dispersion can cause problems for some applications. For example, quantum cryptography schemes implementing phase or phase-and-time coding rely on photons arriving at well defined times, i.e. well localized in space. In dispersive media, like optical fibres, different group velocities are a source of noise for the localization of the photons; for this reason the broadening of the photon bandwidth must be circumvented or controlled [4].

In our device the spectral width of the signal and idler is indeed given by

$$\Delta\omega = 5.57 \frac{1}{|\frac{1}{v_{gS}} + \frac{1}{v_{gI}}|L}$$

where v_{gS} and v_{gI} are the signal and idler group velocities at perfect phase matching. For the above AlGaAs structure, we obtain a bandwidth of about 0.3 nm. We notice that, in copropagating geometry, the sum of the group velocities is replaced by their difference in the previous expression, thus increasing the spectral width.

Therefore, the interesting figure of merit for this kind of structure is the signal and idler generation efficiency per unit of bandwidth (W W^{-1} nm^{-1}), for each interaction. The

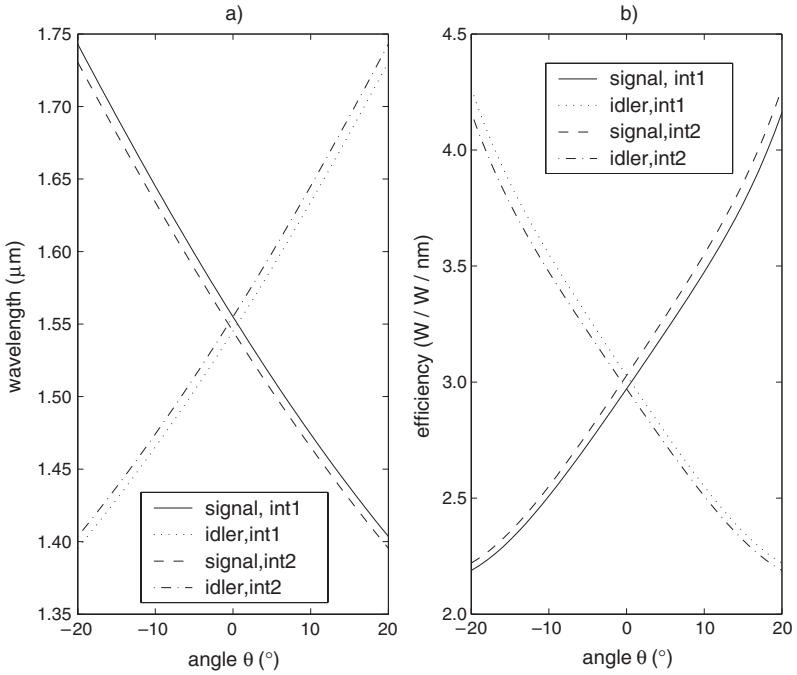

Figure 9. Signal and idler wavelengths (a) and PF efficiency (b) versus angle of incidence for the structure reported in the text. The values obtained for both interactions 1 and 2 are reported.

numerical results for the present AlGaAs waveguide are plotted in figure 9.

The sample modelled in this section has been fabricated and characterized by performing effective index and surface-emitting second harmonic generation measurements. This work has confirmed the compliance with design specifications on phase matching wavelength and parametric gain; the results are given in [18].

Finally, another interesting advantage of this scheme is that the combination of type II phase matching with counterpropagation for the signal and the idler leads naturally to polarization entanglement, as in the polarization-entangled photon pair source of Kwiat *et al* [21]. The photon pair is generated in a superposition of the states produced by interaction 1 and 2. The weight of each of those states in the total state vector is related to the efficiency of the corresponding interaction. Namely, after removal of the vacuum component, it can be written as

$$|\mathrm{ent}\rangle = \frac{\eta_1}{\sqrt{|\eta_1|^2 + |\eta_2|^2}} |\bar{\omega}_{\mathrm{S},1}, \mathrm{TE}\rangle |\bar{\omega}_{\mathrm{I},1}, \mathrm{TM}\rangle + \frac{\eta_2}{\sqrt{|\eta_1|^2 + |\eta_2|^2}} |\bar{\omega}_{\mathrm{S},2}, \mathrm{TM}\rangle |\bar{\omega}_{\mathrm{I},2}, \mathrm{TE}\rangle$$

where $|\eta_{\mathrm{i}}|^2$ may be regarded as the efficiency of interaction i expressed in photon pairs per pump photon [18].

5. Discussion and comparative analysis

So far we have presented the results we obtained until recently in the realization of twin photon semiconductor sources by using three different phase matching schemes.

Now we want to discuss and compare the characteristics and performances of the devices presented in the previous sections. A summary of this discussion is given in table 1.

The first characteristic we want to point out is whether the source is an active or a passive device. In the case of form birefringence, the need for a pair of materials with a sufficient index contrast leads to the oxidation of the AlAs layers; therefore, due to the insulating nature of the oxide, it is not possible to have an electrical transport within the structure. We can possibly consider the option of an optical pumping, but a deep investigation is necessary to ensure that the proximity of the Alox is not a problem for the radiative efficiency of the emitters. For these reasons, the form birefringent device presented in this paper is passive. The whole design of our mode matched device is conceived such as to result in an active structure: laser emission and parametric down-conversion occur on the same chip. Our actual studies on counterpropagating signal and idler geometry, conversely, involve an external laser pump; a development of this device, including a VCSEL on the top of the waveguide, can be envisaged [22]. In this case the emitted photons will have a fixed wavelength as the angle of incidence would be fixed.

The twin photon wavelength range of the three devices described is linked to the transparency range for the materials used, the availability of pump source wavelength and the phase matching condition. The transparency range for AlGaAs is very broad: the limits are given by the phononic resonance (around 30 μm) and by the band gap energy. The direct band gap energy at room temperature goes from 1.42 eV (∼870 nm) for GaAs to 2.8 eV (∼443 nm) for AlAs [23]. In the domain of twin photon applications the devices realized up to now are thus well suited to the production of twin photons in the telecommunications range, for fibre transmissions. In the case of counterpropagating geometry we have also investigated the feasibility of a source for the silicon absorption band, for line-of-sight experiments in quantum key distribution. Numerical simulations show that a ZnSe/ZnMgSe structure would have the same overall efficiency as the AlGaAs structure.

Table 1. Synopsis of the characteristics and performances of the devices presented in this paper.

Type of phase matching	Form birefringence	Modal phase matching	Counterpropagating signal and idler phase matching
Active/passive device	Passive (end fire coupling)	Active	Passive (easy top coupling)
Twin photon wavelength (realized)	2.1 μm (exp)	1.55 μm (exp)	1.55 μm (exp)
Twin photon wavelength (possible)	1.55 μm	1.55 μm	0.8–1.55 μm
Signal spectral width at degeneracy	$\sim$150 nm(exp)	$\sim$120 nm (th.)	$\sim$0.3 nm (th.)
PF efficiency	$\sim 6 \times 10^{-6}$ W W^{-1} cm^{-2} (exp)	$\sim 6 \times 10^{-7}$ W W^{-1} cm^{-2} (th.)	$\sim 1 \times 10^{-13}$ W W^{-1} (th.)
Optical losses (TE polarization)	1 cm^{-1} (at 2.1 μm) (exp)	0.1 cm^{-1} (at 1.55 μm) (exp)	1.4 cm^{-1} (1.55 μm) (exp)
Sensitive parameter for phase matching wavelength	Thickness of GaAs layer Refractive index of Alox (th.)	Thickness of $Al_{0.25}Ga_{0.75}As$ layers (th.)	Very stable and easy tunable (th.)

As regards the parametric efficiency of the three devices, a few remarks are in order: in the two cases of copropagating signal and idler (form birefringence and modal phase matching) the efficiency depends quadratically on the sample length L, which explains why the efficiency is normalized to L^2 in table 1. In the case of counterpropagating signal and idler, in contrast, the efficiency does not depend on L (of course with this reasoning optical losses are not taken into account). Another discriminating issue is the bandwidth of the generated signal; the counterpropagating geometry allows us to generate a spectrally narrow signal, which we emphasize as an important advantage compared with what is obtained in the copropagating geometry. We notice that the greater refractive index dispersion of semiconductor materials with respect to usual nonlinear crystals makes the phase matching resonance narrower in the semiconductor case. The bandwidth values obtained in this paper for the three configurations are in the same range as those obtained in [18] for PPLN.

Another important characteristic for quantum information applications is the closeness of the generated photons to the Fourier transform limit. In the hypothesis of creation of a one photon state that is the coherent superposition of one photon states within the spectral width of the phase matching, we can find a rough estimate of this. For a 1 mm waveguide, taking into account the spectral width of the process and the emission time uncertainty due to the length of the sample, we find that photons are less than 1.5 times over the Fourier transform limit in the counterpropagating geometry, whereas in the copropagating geometry they are around 200 times over the Fourier transform limit.

Optical losses are another crucial characteristic our devices: in quantum optics applications, optical losses correspond to events of disappearance of one photon of the pair. The remaining photon is useless and becomes a source of noise. The method we generally use to measure propagation losses in semiconductor waveguides is based on Fabry–Perot transmission fringes, and is well established for single mode optical waveguides. We have recently proposed an extension of this technique to the case of multimode and tightly confining semiconductor waveguides [24]. This procedure involves Fabry–Perot measurements on a large spectral range, in order to find an interval where multimode effects do not alter the loss measurements. The validity domain of this method does not include form birefringent samples; the loss measurement reported in table 1 was obtained with a scattering technique using femtosecond pulses [25].

For the three kinds of devices, optical ridges are defined by chemical etching; the high value of losses found in the counterpropagating geometry (1.4 cm^{-1}) is due to a too high aluminium content of the structure: the natural Al oxidation induces higher losses and problems in the sample cleavage. A new structure with a lower Al content is actually under study and should give the same loss value as the one obtained for modal phase matching heterostructures. In form birefringent samples, the losses (1 cm^{-1}) have two main origins: scattering (especially at the interface with the oxide) and two photon absorption. This loss level corresponds to a percentage of 'broken' pairs of 20% for a sample of length $L = 1$, mm and of 80% for $L = 5$ mm. In modal phase matched samples the losses are lower (0.1 cm^{-1}); the measurement has been carried out on a non-doped sample. In this case the percentage of 'broken' pairs is 2% when $L = 1$ mm, and 10% when $L = 5$ mm.

In order to choose among the possible quantum optics experiments which could be performed with these sources, it is important to know the quantum state of the generated fields: in the case of form birefringence and modal phase matching, we could describe the emitted field state as $|\Psi\rangle = \int \mathrm{d}\omega_S\, f(\omega_S)|\bar{\omega}_S, \mathrm{TE}\rangle|\omega_P - \bar{\omega}_S, \mathrm{TM}\rangle$. This provides a pair of twin photons that can be used, for example, in single photon, quantum cryptography protocols (using the twin photon to trigger the detector) or in photon pair protocols (energy–time or time–bin entanglement).

In the case of counterpropagating photons the emitted field state is

$$|\mathrm{ent}\rangle = \frac{\eta_1}{\sqrt{|\eta_1|^2 + |\eta_2|^2}}|\bar{\omega}_{S,1}, \mathrm{TE}\rangle|\bar{\omega}_{I,1}, \mathrm{TM}\rangle + \frac{\eta_2}{\sqrt{|\eta_1|^2 + |\eta_2|^2}}|\bar{\omega}_{S,2}, \mathrm{TM}\rangle|\bar{\omega}_{I,2}, \mathrm{TE}\rangle.$$

In this case, the entanglement can be obtained for three variables: energy, momentum and polarization. More complex experimental set-ups (e.g. the illumination of the sample through an appropriate diffraction grating) allow one to directly obtain the Bell states [17]; this would allow one to perform Bell's inequality tests on the photons emitted by this source.

Finally, another important point for our devices is an analysis of how parameter variations in the structure (layer thicknesses, alloy composition, refractive indices) influence the parametric tuning curves. This analysis is important for any practical design, and to assess the tolerances in growth steps and in knowledge of the refractive indices.

The results given here are obtained by performing numerical simulations in the planar waveguide approximation, which is quite satisfactory as long as the ridge is wider than 5 μm.

For each of the three devices, we have looked for the most sensitive parameter for frequency conversion. In the case of form birefringent structures the thickness of GaAs layers has to be controlled most homogeneously: a 1% relative variation of the thickness induces a 6 nm shift of the pump wavelength at degeneracy [26]. Another crucial point for these structures is the precise knowledge of the Alox refractive index, which depends on the oxidation conditions (oxidation time and temperature, thickness of AlAs layers,...). A variation of 0.03 of this index can induce a shift of 10 nm from the degenerate pump wavelength. The modal phase matched structures are grown by realizing a superlattice; the MBE cells contain GaAs, AlAs and $Al_{0.25}Ga_{0.75}As$: all the alloys of the structure are blended by conveniently adjusting the flux of these cells. We have thus investigated the sensitivity of the structure to relative variations of thickness and concentration of the different layers, finding that the most critical parameter is the thickness of $Al_{0.25}Ga_{0.75}As$ layers: a 1% variation of this parameter induces a 2.5 nm shift of the degenerate pump wavelength.

As regards the counterpropagating geometry our calculations show that the structure is very stable with respect to the variation of both thickness and composition of the layers; the most sensitive parameter is aluminium concentration: as an example, a relative variation of 5% induces a variation in the signal wavelength of 0.1%, for an angle of incidence of 20°.

In conclusion, in this paper we have illustrated our recent advances in the realization of twin photon semiconductor sources. Three kinds of sources have been presented and compared; their different characteristics allow us to choose the most well adapted device, according to the application envisaged.

Acknowledgments

This work was funded by the European Union through the Projects OFCORSE II, QUCOMM and RAMBOQ.

References

[1] Bowmeester D, Ekert A and Zeilinger A 2000 *The Physics of Quantum Information* (Berlin: Springer)
[2] Bowmeester D, Pan J W, Mattle K, Eibl M, Weinfurter H and Zeilinger A 1997 *Nature* **390** 575
[3] Jennewein T, Weihs G, Pan J W and Zeilinger A 2002 *Phys. Rev. Lett.* **88** 017903
[4] Gisin N, Ribordy G, Tittel W and Zbinden H 2002 *Rev. Mod. Phys.* **74** 145
[5] Sergienko A V and Jaeger G S 2002 *Contemp. Phys.* **74** 145
[6] Tanzilli S, Tittel W, De Riedmatten H, Zbinden H, Baldi P, De Micheli M, Ostrowsky D B and Gisin N 2002 *Eur. Phys. J.* D **18** 155
[7] Van der Ziel J 1975 *Appl. Phys. Lett.* **26** 60
[8] Dellesasse J M, Holonyak J N, Sugg A R, Richard T A and El-Zein N 1990 *Appl. Phys. Lett.* **57** 2844
[9] Fiore A, Berger V, Rosencher E, Bravetti P and Nagle J 1998 *Nature* **39** 463
[10] Fiore A, Berger V, Rosencher E, Bravetti P, Laurent N and Nagle J 1997 *Appl. Phys. Lett.* **71** 3622
[11] Fiore A, Yanz S, Delobel L, Van der Meer P, Bravetti P, Berger V, Rosencher E and Nagle J 1998 *Appl. Phys. Lett.* **72** 2942
[12] De Rossi A, Berger V, Calligaro M, Leo G, Ortiz V and Marcadet X 2001 *Appl. Phys. Lett.* **79** 3758
[13] Gehrsitz S, Reinhart F K, Gourgon C and Herres N 2000 *J. Appl. Phys.* **87** 7825
[14] De Rossi A, Semaltianos N, Berger V, Chirlias E, Vinter B and Ortiz V 2002 *Appl. Phys. Lett.* **80** 4690
[15] De Rossi A, Ortiz V, Calligaro M, Vinter B, Nagle J, Ducci S and Berger V 2004 *Semicond. Sci. Technol.* **19** L99
[16] Ducci S, Lanco L, Berger V, De Rossi A, Ortiz V and Calligaro M 2004 *Appl. Phys. Lett.* **84** 2974
[17] De Rossi A and Berger V 2002 *Phys. Rev. Lett.* **88** 043901
[18] Booth M C, Atatüre A, Di Giuseppe G, Saleh B E A, Sergienko A V and Teich M 2002 *Phys. Rev.* A **66** 023815
[19] Ravaro M, Seurin Y, Ducci S, Leo G, Berger V, De Rossi A and Assanto G 2005 *J. Appl. Phys.* submitted
[20] Ducci S, Berger V, De Rossi A, Leo G and Assanto G 2005 Integrated twin-photon sources for the Si absorption band *J. Opt. Soc. Am.* B submitted
[21] Kwiat P G *et al* 1995 *Phys. Rev. Lett.* **75** 4337
[22] Ding Y J, Khurgin J B and Lee S J 1995 *IEEE J. Quantum Electron.* **31** 1648
[23] Adachi S 1993 *Properties of Gallium Arsenide* ed S Adachi (London: INSPEC)
[24] De Rossi A, Ortiz V, Calligaro M, Lanco L, Ducci S, Berger V and Sagnes I 2005 *J. Appl. Phys.* **97** 073105
[25] Venugopal Rao S, Moutzouris K, Ebrahimzadeh M, De Rossi A, Gintz G, Calligaro M, Ortiz V and Berger V 2002 *Opt. Commun.* **213** 223
[26] De Rossi A, Berger V, Leo G and Assanto G 2005 Birefringence phase matching: tuning and tolerances *IEEE J. Quantum Electron.* submitted